Biochemistry

 Volume 33, Number 43 November 1, 1994

Accelerated Publications

Projection Structure of the CHIP28 Water Channel in Lipid Bilayer Membranes at 12-Å Resolution†

A. K. Mitra*,‡ and M. Yeager‡,§

Department of Cell Biology, The Scripps Research Institute, and Division of Cardiovascular Diseases, Scripps Clinic and Research Foundation, 10666 North Torrey Pines Road, La Jolla, California 92037

A. N. van Hoek,∥ M. C. Wiener,⊥ and A. S. Verkman∥

Departments of Medicine and Physiology, Cardiovascular Research Institute, and Department of Biophysics and Biochemistry, University of California, San Francisco, San Francisco, California 94143

Received June 20, 1994; Revised Manuscript Received August 25, 1994®

ABSTRACT: Osmotic water transport across plasma membranes in erythrocytes and several epithelial cell types is facilitated by CHIP28, a water-selective membrane channel protein. In order to examine the structure of CHIP28 in membranes, large (1.5–2.5-μm diameter), highly ordered, two-dimensional (2-D) crystals of purified and deglycosylated erythrocyte CHIP28 were generated by reconstitution of detergent-solubilized protein into synthetic lipid bilayers via detergent dialysis. Fourier transforms computed from low-dose electron micrographs of such crystals preserved in negative stain display order to 12-Å resolution. The crystal lattice is tetragonal ($a = b = 99.2 \pm 1.4$ Å) with plane group symmetry $p4g$. A projection density map at 12-Å resolution defines the molecular boundary and organization of the CHIP28 monomers in the membrane plane. The unit cell contains four CHIP28 dimers, each composed of two oblong-shaped (37 × 25 Å) monomers with opposite orientations. The CHIP28 monomers associate to form tetrameric structures around the 4-fold axes normal to the membrane plane where stain is excluded. The 2-D crystals of CHIP28 display order extending beyond the limit typically achieved by negative staining and therefore may be amenable to high-resolution structure analysis by cryo-electron microscopy.

Specialized "water channels" have been implicated to account for rapid water transport across plasma membranes in erythrocytes and several epithelial cell types (Finkelstein, 1987). CHIP28[1] (channel-forming integral protein of 28 kDa) is a partially glycosylated membrane protein expressed in erythrocytes and several water-transporting tissues. It functions as a water-selective channel [for reviews, see Agre et al. (1993) and Verkman (1993)] that excludes small ions and solutes (Preston et al., 1992; van Hoek & Verkman, 1992; Zeidel et al., 1992; Ma et al., 1993). CHIP28 is a member of the MIP (major intrinsic protein of the mammalian eye lens; Gorin et al., 1984) superfamily of proteins (Baker & Saier, 1990) that include other homologous water channels of mammalian tissues (Fushimi et al., 1993; Hasegawa et al., 1994) and various channel-forming proteins from prokaryotes and eukaryotes (Pao et al., 1991).

† This work was supported by NIH Grants DK35124 (A.S.V.), AI31535 (M.Y.), and HL48908 (M.Y.), the Gustavus & Louise Pfeiffer Research Foundation (M.Y.), Grants-in-Aid from the National Center of the American Heart Association (AHA) (A.S.V. and M.Y.) and from the California Affiliate of the AHA (A.N.v.H.), and a grant from the academic senate of UCSF (A.N.v.H.). M.C.W. is a Johnson and Johnson fellow of the Life Sciences Research Foundation. A.S.V. and M.Y. are Established Investigators of the AHA, and M.Y. is also supported by Bristol-Myers Squibb.

* Author to whom correspondence should be addressed: telephone, 619-554-4233; FAX, 619-554-6945; E-mail, Mitra@riscem.scripps.edu.

‡ Department of Cell Biology, The Scripps Research Institute.

§ Division of Cardiovascular Diseases, Scripps Clinic and Research Foundation.

∥ Departments of Medicine and Physiology, Cardiovascular Research Institute, UCSF.

⊥ Department of Biophysics and Biochemistry, UCSF.

® Abstract published in *Advance ACS Abstracts,* October 1, 1994.

[1] Abbreviations: CHIP28, channel-forming integral protein of 28 kDa; OG, octyl β-D-glucopyranoside; DOPC, dioleoylphosphatidylcholine; 2-D, two-dimensional; 3-D, three-dimensional.

0006-2960/94/0433-12735$04.50/0

The N- and C-terminal halves of CHIP28 are sequence-related internal repeats. Circular dichroism spectroscopy, Fourier transform infrared spectroscopy, and hydropathy analysis suggest multiple α-helical membrane-spanning domains as well as elements of β-sheet and β-turn (van Hoek et al., 1993a). Localization studies of a reporter domain attached to CHIP28 indicate four principal membrane-spanning domains and a cytoplasmic orientation of the N- and C-termini in the endoplasmic reticulum (Skach et al., 1994). However, proteolysis studies of epitope-tagged CHIP28 constructs in oocyte membranes suggest that the polypeptide chain crosses the bilayer six times (Preston et al., 1994). Electron micrographs of rotary-shadowed, freeze-fractured proteoliposomes reconstituted with CHIP28 and of cells expressing CHIP28 suggest that CHIP28 forms tetramers in the bilayer (Verbavatz et al., 1993). Several lines of evidence suggest that CHIP28 monomers function as individual water channels: radiation inactivation studies on water transport in native membranes (van Hoek et al., 1991), water-transport properties of oocytes expressing wild-type and mutant CHIP28 mixtures (Preston et al., 1993; Zhang et al., 1993), and heterodimers comprised of wild-type and mutant subunits (Shi et al., 1994).

The biochemical and biophysical data available to date do not reveal what structural elements constitute and control the water-selective permeability of CHIP28. For this purpose a knowledge of the high-resolution three-dimensional (3-D) structure in the membrane bilayer is essential. Two-dimensional crystals of membrane proteins have been found to be extremely useful for determining detailed 3-D structures of membrane proteins (Henderson et al., 1990; Jap et al., 1991; Kühlbrandt et al., 1994). CHIP28 from human erythrocytes was purified in the detergent octyl β-D-glucopyranoside (OG), deglycosylated, and then reconstituted with lipids by slow dialysis to generate highly ordered 2-D crystals. Image processing of electron micrographs yielded a 12-Å-resolution density map that reveals the molecular boundary and organization of CHIP28 monomers in the plane of the membrane bilayer.

EXPERIMENTAL PROCEDURES

Protein Purification. Native, partially glycosylated CHIP28 was purified as described (van Hoek et al., 1993a). A homogeneous protein preparation of deglycosylated CHIP28 was prepared by treatment with recombinant PNGase F (NEB, Beverly, MA) followed by Q-Sepharose chromatography (van Hoek et al., 1993b). In a sizing column, the purified protein migrates as a monomer. On the basis of osmotic permeability measurements, deglycosylated CHIP28 retained its water-transporting activity when reconstituted into liposomes (Zhang et al., 1993; data not shown).

Two-Dimensional Crystallization. Two-dimensional crystallization of CHIP28 in lipid bilayer membranes was accomplished by lipid–protein reconstitution via slow detergent dialysis [Mitra et al., 1993; for reviews, see Jap et al. (1992) and Kühlbrandt (1992)]. Purified and deglycosylated CHIP28 at concentrations of 2–4 mg/mL (as estimated using the Lowry assay) in 20 mM sodium phosphate, 0.1 mM EDTA, and 100 mM NaCl, pH 7.0, containing 35 mM octyl β-D-glucopyranoside (OG) (Anatrace, Maumee, OH) was mixed with a solution of dioleoylphosphatidylcholine (DOPC) (Avanti Polar Lipids, Birmingham, AL) in OG containing 20 mM sodium phosphate, 0.1 mM EDTA, 100 mM NaCl, and 0.025% NaN_3, pH 7.0, at a lipid to protein ratio of 1:1–1:3 (w/w). Mixtures were contained in microdialysis chambers constructed from the caps of 0.6-mL plastic Eppendorf tubes (volume 50–100 μL) and were dialyzed (SpectraPor, MWCO 12–14 kDa) at 27 °C for 6–8 days against 1 L of detergent-free buffer with four to five buffer changes, thereby minimizing the detergent concentration.

Electron Microscopy and Image Analysis. An aliquot (2–4 μL) of the reconstituted sample was allowed to adhere for 90 s to an electron microscope grid coated with collodion-supported carbon film that had been rendered hydrophilic by glow discharging. The grid was successively washed three times for 5 s with 100-μL drops of distilled water, stained twice for 25 and 45 s with 5-μL drops of uranyl formate (Sigma, St. Louis, MO) prepared according to Williams (1981), blotted with filter paper to remove excess solution, and then air-dried. The grids were examined in a Philips CM12 electron microscope operated at 100 kV. Images recorded on Kodak SO163 film using low-dose conditions ($\sim$10 e/Å^2) at a magnification of 45 900 and at $\sim$400–700 nm underfocus were developed in full-strength Kodak D19 for 10 min. The magnification was calibrated using the 173.5-Å lattice spacing of negatively stained catalase crystals (Unwin, 1975). Micrographs were screened by optical diffraction, and five crystalline areas were selected from five micrographs that showed the sharpest diffraction spots to the highest resolution. These areas were digitized on a PDS Perkin-Elmer flat-bed microdensitometer with step and aperture sizes of 20 μm, corresponding to 4.7 Å on the specimen.

Image processing of the digitized $\sim 1200 \times 1300$ pixel areas was performed using the MRC suite of programs (Amos et al., 1982; Henderson et al., 1990). For this purpose the optical density values were floated and padded to 1024×1024 or 2048×2048 pixels, and Fourier transforms were computed. The reciprocal lattice parameters were refined by least-squares minimization of the difference between observed and calculated positions of the reflections. The "lattice-unbending" technique described in Henderson et al. (1990) was used to correct for distortions in the lattice using the program system SPECTRA (Schmid et al., 1993). In this method cross-correlation analysis is used to correct for the lattice distortions, and the corrected phases and amplitudes at the reciprocal lattice points were computed from the Fourier transform of the unbent image. The amplitudes of the reflections in the computed transforms were scaled such that the averaged amplitude in each transform was the same. Reflections beyond $\sim$15-Å resolution that were located between the first and the second contrast transfer nodes were corrected for phase reversal. Using the scaled amplitudes, and after aligning the images to a common phase origin, the merged phases $\langle\varphi\rangle$ and amplitudes $\langle|F|\rangle$ were calculated as

$$\langle\varphi\rangle = \tan^{-1}\{(\sum|F_i|\sin\varphi_i)/(\sum|F_i|\cos\varphi_i)\} \quad (1)$$

$$\langle|F|\rangle = (1/N)\{(\sum|F_i|\sin\varphi_i)^2 + (\sum|F_i|\cos\varphi_i)^2\}^{1/2} \quad (2)$$

where N (=5) is the total number of sets of calculated phases and amplitudes that were merged. Merged phases and amplitudes of reflections up to 12-Å resolution were used to calculate the projected reconstructions. The figure of merit m of a reflection and its symmetry mates was calculated as the cosine of the mean value of the deviations of the phase angles from 0° or 180°. The amplitudes were weighted by these figures of merit for calculating the symmetry-imposed map, and the expected noise level $\Delta\rho$ is given by (Dickerson et al., 1968)

$$\Delta\rho^2 = \sum_{hk}|F|^2(1.0 - m^2) + \delta^2 \quad (3)$$

where δ is the standard deviation in the symmetry-averaged amplitude.

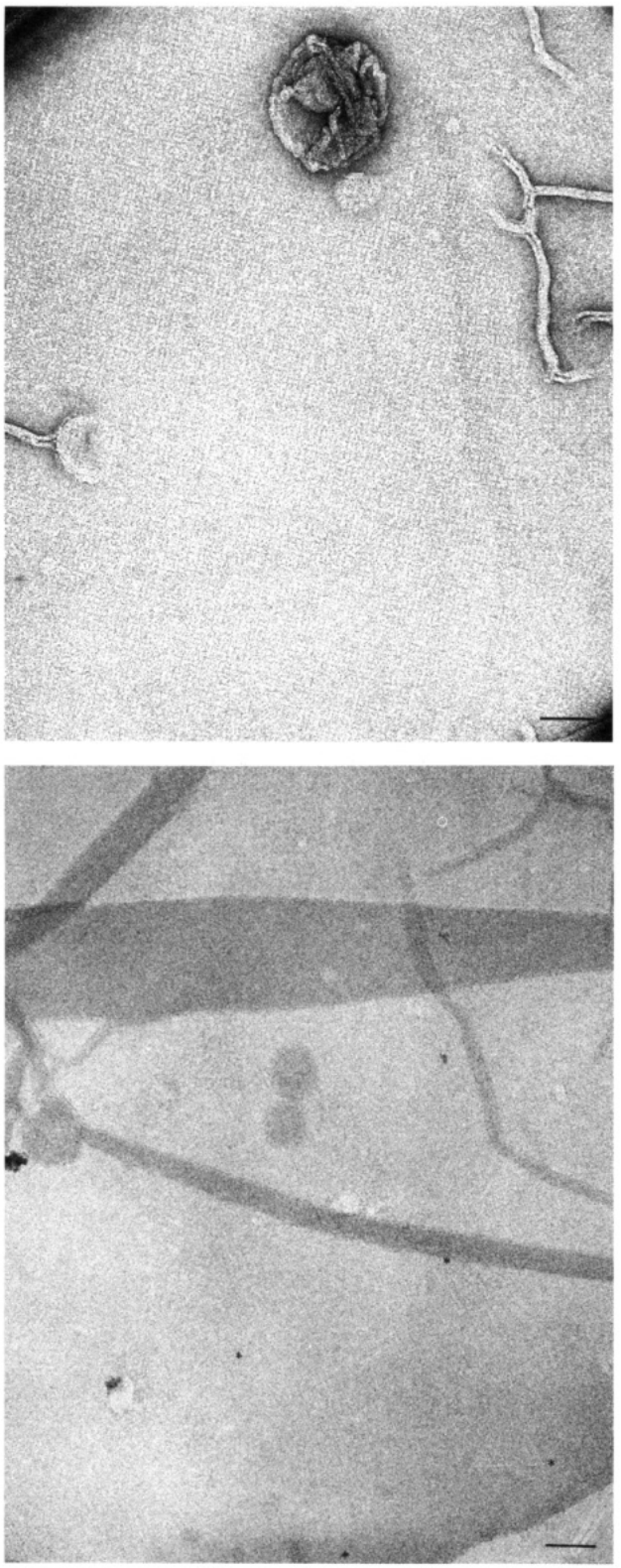

FIGURE 1: Electron micrographs of nominally untilted 2-D crystals of CHIP28 stained with uranyl formate. (a, top) High-dose image recorded at ~2.0 μm underfocus where the rectangular lattice due to the enhancement of low-resolution features by phase contrast can be seen. (b, bottom) Low-dose image recorded closer to focus (~0.5 μm underfocus) where the rectangular lattice is just barely visible. The area demarcated by asterisks was digitized and processed. Bar: 1000 Å.

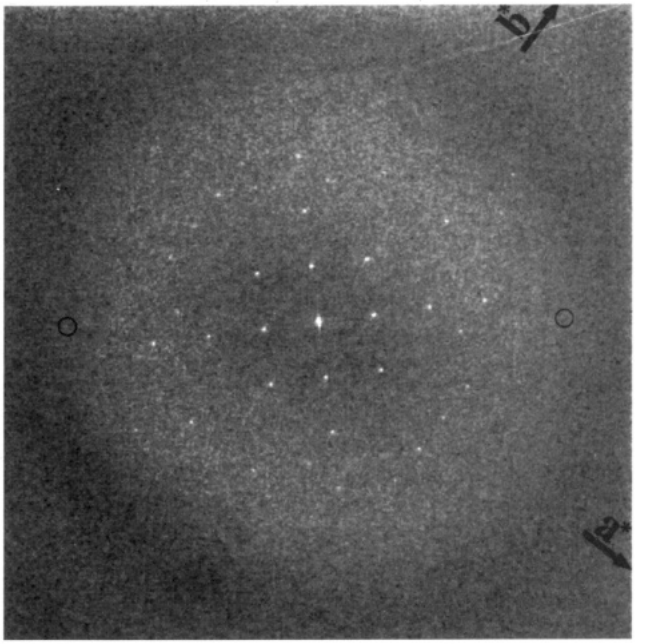

FIGURE 2: Computed Fourier transform obtained directly from a digitized area of an image such as in Figure 1b. The degree of lattice preservation without being corrected for possible lattice disorder is excellent, with crystalline order extending to better than 15 Å. The 5,4 reflection (circled) corresponds to 15.5-Å resolution.

RESULTS AND DISCUSSION

In vitro reconstitution and two-dimensional crystallization of deglycosylated CHIP28 in synthetic lipid bilayer membranes were accomplished by slow detergent dialysis. The lipid-reconstituted CHIP28 samples consist of both sheets and unilamellar vesicles. The proportion of the two varied between experiments with the vesicular fraction increasing with time after completion of dialysis. The crystalline areas (Figure 1) were larger and better ordered in sheets than in the flattened vesicles. Displays of the computed Fourier transforms, even before corrections for lattice distortions, showed diffraction to 15.5-Å resolution (Figure 2). After correction for lattice distortions, significant reflections to 12-Å resolution that agreed with the constraints of the *p*4*g* plane group symmetry were detected in the digitized transform. Therefore, the degree of lattice preservation is excellent. In Figure 2, the 4-fold symmetry normal to the plane of the membrane is apparent. The *h* (=odd), 0, and 0,*k* (=odd) reflections are weak or absent, indicating the presence of in-plane 2-fold screw axes. The phases (φ) at the reciprocal lattice points after suitable origin shifts are close to the centrosymmetric values 0° or 180°. These phase angles and the calculated amplitudes satisfy the constraints of plane group symmetry *p*4*g* (3-D space group $P42_12$) of a tetragonal lattice. Table 1 lists the merged phases and amplitudes for significant reflections, before and after imposing the symmetry constraints of the *p*4*g* plane group.

Figure 3 displays projected density maps of CHIP28 in the membrane at 12-Å resolution generated (a) without imposing symmetry and (b) after imposing *p*4*g* symmetry. The heavy dashed lines delineate the square unit cell (dimensions $a = b = 99.2 \pm 1.4$ Å) containing four dimers of CHIP28. The reconstructions, generated by combining data from a total of ~10 500 unit cells, represent the average of the projected views of 84 000 (10 500 × 8) independent CHIP28 molecules. The unweighted and amplitude-weighted average values of the deviations of the merged phases from centrosymmetric values were 11° and 5°, respectively. These low values allow clear demonstration of the *p*4*g* lattice symmetry (2-fold, 4-fold, and 2_1 screw axes) in the reconstruction in which no symmetry was imposed (Figure 3a).

Around the 4-fold axis there is relatively little stain penetration, and four monomers of CHIP28 belonging to four

Table 1: Averaged Projection Amplitudes and Phases of the CHIP28 Crystal up to 12-Å Resolution before ($\langle|F|\rangle$, $\langle\varphi\rangle$) and after ($|F_s|$, φ_s) Application of *p4g* Plane Group Symmetry[a]

h	*k*	*N*	resoln (Å^{-1})	$\langle\|F\|\rangle$	$\langle\varphi\rangle$	$\|F_s\|$[b]	φ_s	*h*	*k*	*N*	resoln (Å^{-1})	$\langle\|F\|\rangle$	$\langle\varphi\rangle$	$\|F_s\|$[b]	φ_s
0	1	4	99.2	212	35	*c*	*c*	2	−7	2	13.6	173	−15	143 (22)	0
0	1	4	99.2	*d*	*d*	*c*	*c*	2	7	1	13.6	*d*	*d*		180
0	2	5	49.6	3688	178	3855 (118)	180	7	2	1	13.6	112	165		180
2	0	5	49.6	4021	179		180	7	−2	*e*	13.6				0
0	3	3	33.1	367	−2	*c*	*c*	2	−6	2	15.7	307	30	269 (32)	0
3	0	3	33.1	437	165	*c*	*c*	2	6	2	15.7	295	21		0
0	4	5	24.8	798	−175	767 (22)	180	6	2	3	15.7	163	−12		0
4	0	5	24.8	735	179		180	6	−2	4	15.7	309	4		0
0	5	2	19.8	153	41	*c*	*c*	2	−5	5	18.4	583	10	491 (53)	0
5	0	2	19.8	148	−141	*c*	*c*	2	5	5	18.4	370	−172		180
0	6	3	16.5	240	−8	301 (43)	0	5	2	5	18.4	608	−174		180
6	0	2	16.5	361	−16		0	5	−2	5	18.4	401	−9		0
0	7	1	14.2	112	−34	*c*	*c*	2	−4	5	22.2	957	6	695 (149)	0
7	0	2	14.2	175	8	*c*	*c*	2	4	1	22.2	289	37		0
1	−7	3	14.0	195	−33	131 (27)	0	4	2	5	22.2	1039	3		0
1	7	3	14.0	80	−28		0	4	−2	4	22.2	495	14		0
7	1	*e*	14.0				0	2	−3	5	27.5	651	−170	1009 (174)	180
7	−1	3	14.0	119	1		0	2	3	5	27.5	1371	−2		0
1	−6	5	16.3	361	166	298 (31)	180	3	2	5	27.5	672	−13		0
1	6	3	16.3	217	−3		0	3	−2	5	27.5	1341	−178		180
6	1	4	16.3	357	11		0	2	−2	5	27.5	2171	−178	2305 (95)	180
6	−1	2	16.3	257	154		180	2	2	5	27.5	2439	179		180
1	−5	2	19.5	523	3	480 (19)	0	3	−6	1	14.8	171	−137	133 (16)	180
1	5	5	19.5	440	5		0	3	6	4	14.8	115	33		0
5	1	4	19.5	444	17		0	6	3	3	14.8	113	−15		0
5	−1	5	19.5	512	1		0	6	−3	*e*	14.8				180
1	−4	5	24.8	1570	0	1631 (21)	0	3	−5	2	17.0	*d*	*d*	184 (7)	0
1	4	5	24.8	1619	178		180	3	5	4	17.0	168	13		0
4	1	5	24.8	1689	175		180	5	3	2	17.0	*d*	*d*		0
4	−1	5	24.8	1644	2		0	5	−3	1	17.0	173	13		0
1	−3	4	31.4	1175	−10	681 (231)	0	3	−4	4	19.8	503	175	816 (55)	180
1	3	2	31.4	*d*	*d*		0	3	4	5	19.8	1090	−4		0
3	1	5	31.4	1102	−11		0	4	3	4	19.8	512	−9		0
3	−1	2	31.4	*d*	*d*		0	4	−3	5	19.8	1157	179		180
1	−2	2	44.4	*d*	*d*	336 (42)	180	3	−3	5	23.4	2154	−179	2345 (135)	180
1	2	4	44.4	410	0		0	3	3	5	23.4	2536	176		180
2	1	3	44.4	*d*	*d*		0	4	−6	1	13.8	260	134	184 (44)	180
2	−1	3	44.4	336	154		180	4	6	*e*	13.8				180
1	−1	5	70.1	4521	−179	4376 (103)	180	6	4	2	13.8	91	−163		180
1	1	5	70.1	4231	179		180	6	−4	1	13.8	200	−132		180
2	−8	2	12.0	*d*	*d*	125 (13)	0	4	−5	4	15.5	161	170	286 (40)	180
2	8	2	12.0	163	−9		0	4	5	3	15.5	300	−2		0
8	2	2	12.0	98	−8		0	5	4	3	15.5	367	0		0
8	−2	2	12.0	114	−22		0	5	−4	2	15.5	316	178		180
								4	−4	5	17.5	422	−178	485 (44)	180
								4	4	2	15.5	547	−170		180

[a] All reflections that had at least one significant symmetry mate are listed. Entries in columns 5 and 6 were used to synthesize the map in which no symmetry was imposed (Figure 3a) while those in columns 7 and 8 were used to synthesize the symmetry-enforced map (Figure 3b). [b] The symmetry-averaged amplitude, and its standard deviation in parentheses, is indicated only once for each group of symmetry-related reflections. [c] Systematic absence. [d] The averaged amplitudes for these reflections were less than the averaged background, and/or the averaged phase differed by more than 50° from 0° or 180°. The amplitude was assigned the averaged background for calculating $|F_s|$, and the phase deviation was assigned 50° for calculating the mean figure of merit. [e] The amplitudes for these reflections were less than the local background in all the data sets. The low values may reflect stain-induced artifacts since symmetry-related mates have significant amplitudes.

dimers form a tetramer (Figure 3b). One such tetramer is encircled by dots. In the view projected onto the membrane plane, the CHIP28 monomer has an oblong shape measuring ~37 × 25 Å. Two monomers, oriented in opposite directions with respect to the membrane plane, contact each other across the 2-fold axis forming a dimer (Figure 3b). Thus, four of the eight molecules in the unit cell are oriented up, and the other four are oriented down. In intact erythrocyte membranes water is transported equally well from either side of the bilayer by CHIP28 molecules that are oriented with their N- and C-termini in the cytoplasm (Zhang et al., 1993). Thus, the artificial up-and-down orientations of monomers *in vitro* in the 2-D crystals should not affect the water transport efficiency. Such asymmetry in molecular orientations is a consequence of the detergent-mediated reconstitution process where factors that determine correct insertion *in vivo* are absent. *In vitro* asymmetric orientations have been noted, for instance, in the case of bacteriorhodopsin (Baldwin & Henderson, 1984; Mitra & Stroud, 1990; Michel et al., 1980) and in the case of cytochrome oxidase (Valpuesta et al., 1990). Such up-and-down orientations (with a similar packing arrangement as in this study) were also observed *in vivo* in 2-D crystals of the chloride pump halorhodopsin (Havelka et al., 1994) isolated from the overexpressing *Halobacterium halobium* strain D2.

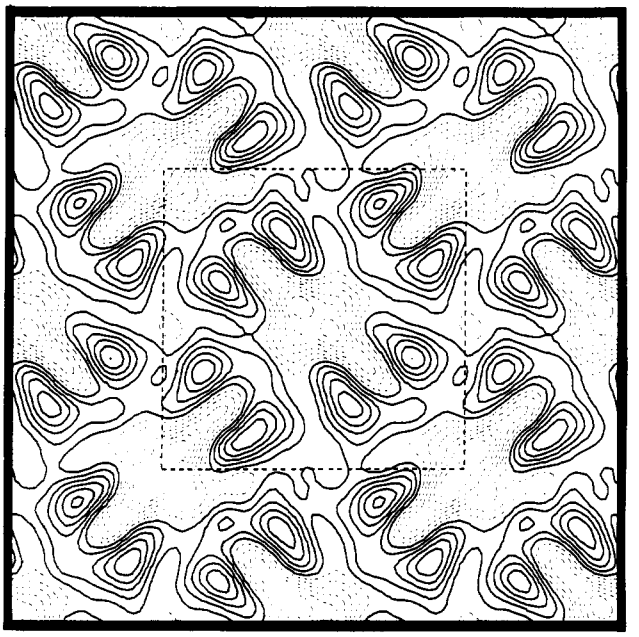

a

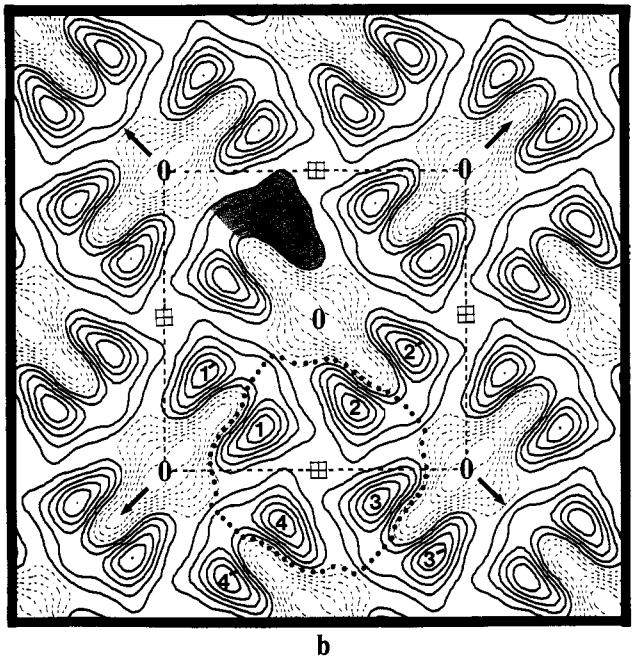

b

FIGURE 3: Averaged projection density map at 12-Å resolution of CHIP28 in the lipid bilayer (a) without applying symmetry and (b) after imposing *p4g* symmetry. The continuous contours represent stain-excluding protein, and the dashed contours represent stain-including lipid areas. The square unit cell ($a = b = 99.2$ Å; heavy dashed lines) contains four dimers. Also shown are the 2-fold axes (0) inclined 45° to the cell edges and the 4-fold axes (crossed box) normal to the membrane plane. The 2_1 screw axes are parallel to the unit cell edges and intersect these at 1/4 and 3/4. A monomer is shaded, and a tetramer is encircled by dots. Monomers have the same orientation in a tetramer but are oppositely oriented in dimers; e.g., 1 (up) and 1′ (down), 2 (up) and 2′ (down). The estimated noise level in panel b calculated using eq 3 is ~20% of the density increment between the contour levels.

The projected area of a CHIP28 tetramer is ~3320 Å^2, similar to the value obtained from electron micrographs of rotary-shadowed, freeze-fractured samples (Verbavatz et al., 1993). The area covered by the CHIP28 molecule in projection is ~830 Å^2 and could readily accommodate either four or six α-helices oriented normal to the membrane plane as predicted by studies on the membrane topology of CHIP28 (Preston et al., 1994; Skach et al., 1994). Using a bilayer thickness of 40 Å and a protein partial specific volume of 0.77 cm^3/g, the volume occupied by a monomer is ~33 400 Å^3, similar to the expected volume of 36 400 Å^3 for a protein of 28 kDa molecular mass. The total area covered by lipid in the unit cell is ~3200 Å^2. On the basis of a value of 59 Å^2 for the area per DOPC headgroup in synthetic bilayers at 66% relative humidity (Wiener & White, 1992) or a value of 64 Å^2 per lipid headgroup in biological membranes (Yeager et al., 1980), there are ~108 or ~100 lipid molecules in the unit cell. These values correspond to ~14 or ~12 lipid molecules per CHIP28 molecule. In comparison, the observed numbers of lipid molecules per protein molecule in 2-D crystals of other membrane proteins are, for instance, ~9 for bacteriorhodopsin (Miercke et al., 1989) and halorhodopsin (Havelka et al., 1994) and ~28 for LHCII (Kühlbrandt & Downing, 1989).

The projection map of stain (uranyl formate) embedded CHIP28 shows tetrameric contacts around the 4-fold axis and dimeric contacts across the diagonally running in-plane 2-fold axis (Figure 3b). Through the dimeric interaction, each monomer contacts a monomer of the neighboring tetramer; e.g., 1 with 1′, 2 with 2′, etc. (Figure 3b). Relative to the amount of stain (uranyl formate) accumulation in the lipid headgroup regions betweeen tetramers, there is little or no inclusion of stain at the center of the tetramer.

Our 2-D crystals of CHIP28 display the same symmetry as those recently examined by Walz et al. (1994a,b), who also used specimens stained negatively by uranyl formate. Their preparation contained purified native (partially glycosylated) protein, and *Escherichia coli* lipids were used for reconstitution. In comparison to the projection maps of Walz et al. at ~20-Å (Walz et al., 1994a) and at 16-Å resolution (Walz et al., 1994b), our reconstruction at 12-Å resolution (Figure 3b) more clearly delineates the molecular boundary and packing of the monomers. Even when computed at 20-Å or at 16-Å resolution, our map does not show accumulation of stain at the center of the tetramer as observed by these authors. On the basis of the inclusion of stain at the center of the tetramer, Walz et al. (1994a,b) proposed a model in which water pores from each of the four monomers coalesce to produce a water-conducting pathway in the middle of the tetrameric structure that is accessible from the two sides of the bilayer. Our projection map does not show such an "open" configuration and suggests closer packing of the individual monomers at the 4-fold and the 2-fold axes. The difference in glycosylation in the two preparations is probably not sufficient to explain the observed difference in the tetrameric structure. This is because, in native CHIP28, glycosylation is only partial, and short-chain carbohydrates attached by glycosylation are likely to have flexible tertiary structures that would not contribute density in the crystallographically averaged map. In addition, deglycosylation probably does not significantly alter the tertiary structure of CHIP28 because water transport is unaffected (Zhang et al., 1993). Thus, any difference in stain-including mass in the tetramer could reflect rearrangements in the packing of the monomers, possibly due to the influence of the different types of lipids used in 2-D crystallization. The absence of stain near the 4-fold axis could also be due to the presence of residual detergent molecules that may result in variable staining (Lyon & Unwin, 1988). This issue of whether there is a channel at the center of the tetramer should be resolved from higher resolution maps calculated from frozen-hydrated crystals.

The projection density map defines the molecular boundary and packing of CHIP28 monomers (Figure 3b), but elements of secondary structure are not revealed at this resolution.

However, the 2-D crystals display order (12 Å) beyond the limit previously achieved by negative staining (15–20 Å) and therefore may be amenable to high-resolution cryo-electron microscopy using frozen-hydrated specimens.

ACKNOWLEDGMENT

We thank Andy Hoenger and Ron Milligan for assistance in using the SPECTRA suite of programs.

REFERENCES

Agre, P., Preston, G. M., Smith, B. L., Jung, J. S., Raina, S., Moon, C., Guggino, W. B., & Nielsen, S. (1993) *Am. J. Physiol. 265*, F463–F476.

Amos, L. A., Henderson, R., & Unwin, P. N. T. (1982) *Prog. Biophys. Mol. Biol. 39*, 183–231.

Baker, M. E., & Saier, M. H., Jr. (1990) *Cell 60*, 185–186.

Baldwin, J., & Henderson, R. (1984) *Ultramicroscopy 14*, 319–336.

Dickerson, R. E., Weinzierl, J. E., & Palmer, R. A. (1968) *Acta Crystallogr., Sect. B: Struct. Crystallogr. Cryst. Chem. 24*, 997–1003.

Finkelstein, A. (1987) *Water Movement through Lipid Bilayers, Pores, and Plasma Membrane: Theory and Reality*, John Wiley and Sons, New York.

Fushimi, K., Uchida, S., Hara, Y., Hirata, Y., Marumo, F., & Sasaki, S. (1993) *Nature 361*, 549–552.

Gorin, M. B., Yancey, S. B., Cline, J., Revel, J.-P., & Horwitz, J. (1984) *Cell 39*, 49–59.

Hasegawa, H., Ma, T., Skach, W., Matthay, M. A., & Verkman, A. S. (1994) *J. Biol. Chem. 269*, 5497–5500.

Havelka, W. A., Henderson, R., Heymann, J. A. W., & Oesterhelt, D. (1993) *J. Mol. Biol. 234*, 837–846.

Henderson, R., Baldwin, J. M., Ceska, T. A., Zemlin, F., Beckmann, E., & Downing, K. H. (1990) *J. Mol. Biol. 213*, 899–929.

Jap, B. K., Walian, P. J., & Gehring, K. (1991) *Nature 350*, 167–170.

Jap, B. K., Zulauf, M., Scheybani, T., Hefti, A., Baumeister, W., Aebi, U., & Engel, A. (1992) *Ultramicroscopy 46*, 45–84.

Kühlbrandt, W. (1992) *Q. Rev. Biophys. 25*, 1–49.

Kühlbrandt, W., & Downing, K. (1989) *J. Mol. Biol. 207*, 823–828.

Kühlbrandt, W., Wang, D. N., & Fujiyoshi, Y. (1994) *Nature 367*, 614–621.

Lyon, M. K., & Unwin, P. N. T. (1988) *J. Cell Biol. 106*, 1515–1523.

Ma, T., Frigeri, A., Tsai, S.-T., Verbavataz, J.-M., & Verkman, A. S. (1993) *J. Biol. Chem. 268*, 22756–22764.

Michel, H., Oesterhelt, D., & Henderson, R. (1980) *Proc. Natl. Acad. Sci. U.S.A. 77*, 338–342.

Miercke, L. J. W., Ross, P. E., Stroud, R. M., & Dratz, E. A. (1989) *J. Biol. Chem. 264*, 7531–7535.

Mitra, A. K., & Stroud, R. M. (1990) *Biophys. J. 57*, 301–311.

Mitra, A. K., Miercke, L. J. W., Turner, G. J., Shand, R. F., Betlach, M. C., & Stroud, R. M. (1993) *Biophys. J. 65*, 1295–1306.

Pao, G. M., Wu, L.-F., Johnson, K. D., Höfte, H., Chrispeels, M. J., Sweet, G., Sandal, N. N., & Saier, M. H., Jr. (1991) *Mol. Microbiol. 5*, 33–37.

Preston, G. M., Carroll, T. P., Guggino, W. B., & Agre, P. (1992) *Science 256*, 385–387.

Preston, G. M., Jung, J. S., Guggino, W. B., & Agre, P. (1993) *J. Biol. Chem. 268*, 17–20.

Preston, G. M., Jung, J. S., Guggino, W. B., & Agre, P. (1994) *J. Biol. Chem. 269*, 1668–1673.

Schmid, M. F., Dargahi, R., & Tam, M. W. (1993) *Ultramicroscopy 48*, 251–264.

Shi, L.-b., Skach, W. R., & Verkman, A. S. (1994) *J. Biol. Chem. 269*, 10417–10422.

Skach, W. R., Shi, L., Calayag, M. C., Frigeri, A., Lingappa, V., & Verkman, A. S. (1994) *J. Cell Biol. 125*, 803–817.

Unwin, P. N. T. (1975) *J. Mol. Biol. 98*, 235–242.

Valpuesta, J. M., Henderson, R., & Frey, T. G. (1990) *J. Mol. Biol. 214*, 237–251.

van Hoek, A. N., & Verkman, A. S. (1992) *J. Biol. Chem. 267*, 18267–18269.

van Hoek, A. N., Hom, M. L., Luthjens, L. H., de Jong, M. D., Dempster, J. A., & van Os, C. H. (1991) *J. Biol. Chem. 266*, 16633–16635.

van Hoek, A. N., Wiener, M., Bicknese, S., Miercke, L., Biwersi, J., & Verkman, A. S. (1993a) *Biochemistry 32*, 11847–11856.

van Hoek, A. N., Wiener, M. C., Lipniunas, P., Townsend, R. R., Farinas, J., & Verkman, A. S. (1993b) *J. Am. Soc. Nephrol. 4*, 861 (Abstract).

Verbavatz, J.-M., Brown, D., Sabolić, I., Valenti, G., Ausiello, D. A., Van Hoek, A. N., Ma, T., & Verkman, A. S. (1993) *J. Cell Biol. 123*, 605–618.

Verkman, A. S. (1993) *Water channels: A Volume in Molecular Biology Intelligence Series*, R. G. Landes Co., Austin, TX.

Walz, T., Smith, B. L., Zeidel, M. L., Engel, A., & Agre, P. (1994a) *J. Biol. Chem. 269*, 1583–1586.

Walz, T., Smith, B. L., Agre, P., & Engel, A. (1994b) *EMBO J. 13*, 2985–2993.

Wiener, M. C., & White, S. H. (1992) *Biophys. J. 61*, 428–433.

Williams, R. C. (1981) *J. Mol. Biol. 150*, 399–408.

Yeager, M., Schoenborn, B., Engelman, D., Moore, P., & Stryer, L. (1980) *J. Mol. Biol. 137*, 315–348.

Zeidel, M. L., Ambudkar, S. V., Smith, B. L., & Agre, P. (1992) *Biochemistry 31*, 7436–7440.

Zhang, R., van Hoek, A. N., Biwersi, J., & Verkman, A. S. (1993) *Biochemistry 32*, 2938–2941.